Available online at www.sciencedirect.com
ScienceDirect
Energy Procedia 63 (2014) 301 – 321
Energy Procedia

GHGT-12

# Low Energy $CO_2$ Capture Enabled by Biocatalyst Delivery System

John Reardon, Tracy Bucholz, Matthew Hulvey, Jonathan Tuttle, Alex Shaffer, Dawn Pulvirenti, Luke Weber, Keith Killian, and Aleksey Zaks *

*Akermin Inc., 1005 N. Warson Road, Suite 101, Saint Louis, MO 63132-2900, United States of America*

**Abstract**

This work presents research and development progress to improve biocatalysts, solvents, and system integration to reduce the cost of $CO_2$ capture from flue gas. Laboratory data and field demonstration illustrate the potential of biocatalyst-enhanced $CO_2$ capture from coal generated flue gas using non-volatile alkali salt solutions. The first generation biocatalyst system (coated packing) demonstrated 6 to 7-fold enhancement in the volumetric average mass transfer coefficient at 40°C with 3460 hours on coal flue gas with 80% $CO_2$ capture on average. The first 2800 hours operated with an aqueous solution of 20% $K_2CO_3$, and the final 660 hours demonstrated a new higher capacity non-volatile alkaline salt solution (AKM24). Lessons learned from the first generation biocatalyst delivery system (coated packing) demonstration are summarized. A second generation biocatalyst delivery system (biocatalyst microparticles) is introduced that shows a greater potential for rate enhancement in laboratory tests. This new biocatalyst system also provides a lower cost method of biocatalyst addition and replacement on-stream. Preliminary modeling estimates show a total equivalent work less than 220 kWh/t $CO_2$ (including $CO_2$ compression to 150 bar) in two possible process configurations. Preliminary cost analysis demonstrates potential for more than 30% reduction in $CO_2$ capture costs relative to NETL Case 12, version 2 (30% MEA with 75 psig cross over steam, bituminous coal power plant).


Peer-review under responsibility of the Organizing Committee of GHGT-12

*Keywords:* $CO_2$ capture, $K_2CO_3$, AKM24, carbonic anhydrase, enzyme, biocatalyst, non-volatile, post combustion, coal power plant.

## 1. Introduction and Background

Alkaline salt solutions, such as potassium carbonate, have been used in high pressure and temperature syngas and natural gas treating for over half a century [1], but their practicality in low pressure and temperature post combustion

* Corresponding author. Tel.: (314) 669-2619;
*E-mail address:* zaksa@akermin.com


Peer-review under responsibility of the Organizing Committee of GHGT-12
doi:10.1016/j.egypro.2014.11.033

$CO_2$ capture has been limited because of slow kinetics and poor energy performance compared to a benchmark solvent, 30% by weight monoethanolamine (MEA). [2] However, MEA and other alkanolamines present an increased risk of emitting volatile organics and also toxic degradation products.

The significant potential to emit volatile organic compounds (VOCs) in addition to potentially toxic and hazardous air pollutant (HAP) when using conventional amine solvents is a well-reported concern. [3,4,5] For example, Wen and Narula [6] estimated VOC emissions of 3.5 to 7 mg/Nm$^3$ in the form of amine after water wash. Notably, Berglen [7] estimated 16.3 mg/Nm$^3$ as a maximum emission scenario for air dispersion modeling at Technology Centre Mongstad. Moreover, Carter [8] reported as much as 100 ppm VOC emissions in the pilot solvent test unit (PSTU) operating with MEA at the National Carbon Capture Center (NCCC) under non-ideal conditions, which was far above the previously estimated 3 ppm based on MEA vapor after water wash.

While non-volatile alkaline salt solutions can overcome the aforementioned environmental health and safety barriers associated with conventional amine solvents, further development is needed to advance salt-based systems for practical and economic post combustion $CO_2$ capture. First, practical catalysts are needed to accelerate the hydration of $CO_2$. Second, energy efficient process schemes are also needed that integrate efficiently with a steam power cycle to minimize the parasitic energy requirements with $CO_2$ capture. Finally, there is a potential that thermodynamic properties of potassium carbonate solution, a well-studied alkaline salt system, may not provide the energy performance needed for significant reductions in regeneration energy. [2]

This paper summarizes recent research and development efforts to advance biocatalyst systems to increase rate enhancement and to facilitate on-line biocatalyst delivery and make-up; to advance non-toxic, non-volatile, alkali salt solutions for $CO_2$ capture including potassium carbonate ($K_2CO_3$) and a proprietary alkali salt blend (AKM24); and finally to advance process schemes that integrate well with lower temperature steam extraction from coal-fired power plants to reduce equivalent work and costs of $CO_2$ capture.

**Nomenclature**

| | |
|---|---|
| $a$ | Proportionality constant for equilibrium constant correlation |
| $b$ | Temperature coefficient for equilibrium constant correlation |
| $B$ | Generic base, or proton acceptor |
| $C^*_A$ | Equilibrium $CO_2$ concentration in gas phase = $P^*_{CO2}/RT$ |
| $C_A$ | Concentration of $CO_2$, noted as the limiting reagent A, in gas phase of absorber system |
| $d_p$ | Pore diameter (nm) |
| $d_s$ | Solute hydraulic diameter (nm) |
| $D_{bulk}$ | Diffusivity, or diffusion coefficient, for a given solute in bulk solution (m$^2$/s, or cm$^2$/s) |
| $D_{pore}$ | Effective diffusivity of a given solute in the pores of biocatalyst solid (m$^2$/s, or cm$^2$/s) |
| $\phi_{void}$ | Void fraction (gas volume/ total volume), typically with respect to wet operational condition |
| $F_A$ | Mole flow of $CO_2$ in the gas phase at any point in the absorber including exit (kmol/hr, or mol/s). |
| $F_{A0}$ | Mole flow of $CO_2$ in the gas phase as fed to the absorber (kmol/hr, or mol/s) |
| $\Delta F_A$ | Net mole flow of $CO_2$ in the gas phase, captured into the absorber, ($F_{A0}$ - $F_A$) |
| $\Delta H_{abs}$ | Specific heat of absorption (kJ/kg $CO_2$, or kJ/mol $CO_2$) |
| $k_{cat}$ | Enzyme turn over frequency (1/s, or μs$^{-1}$) |
| $k_{cat}/K_M$ | Enzyme pseudo second order rate constant |
| $k_1$ | First order rate constant, or volume average mass transfer coefficient (1/s, or 1/min) |
| $k_g$ | Gas film coefficient |
| $k_g$' | Liquid film coefficient for partial pressure driving force [mmol/(s m$^2$ kPa)] |
| $K_{eq}$ | Equilibrium constant, used to describe vapor-liquid equilibrium of capture solutions |
| $K_G$ | Overall mass transfer coefficient [mmol/(s m$^2$ kPa)], specify packing area or interfacial area basis |
| $K_{Gi}$ | Overall mass transfer coefficient [mmol/(s m$^2$ kPa)], interfacial area basis |
| $K_0$ | Pre-exponential factor in the vapor-liquid equilibrium constant correlation |
| $K_{SP}$ | Solubility product, using molality units |
| $m_i$ | Molality of species-i; for example, $K^+$ (mol $K^+$/kg water), or $HCO_3^-$ (mol $HCO_3^-$/kg water) |

| | |
|---|---|
| $M_{Base}$ | Molecular weight of base salt, for example for $K_2CO_3$ (g/mol) |
| $M_{H2O}$ | Molecular weight of water |
| $pK_{a2}$ | Ionic equilibrium constant for $CO_2$ second acidity in water, expressed as $pK_{a2} = -log_{10}(K_{a2})$ |
| $P^*_{CO2}$ | Equilibrium $CO_2$ partial pressure |
| $Q_{Reb}$ | Reboiler heat duty (GJ/t $CO_2$), or total thermal input required to regeneration capture solution |
| $R_{w0,B0}$ | Ratio of initial water to initial base (equivalent unloaded condition) |
| $T$ | Absolute temperature (Kelvin) |
| $T_{Reb}$ | Reboiler temperature (Kelvin) |
| $x_0$ | Equivalent mass fraction of base in solution in the 'initial' unloaded condition (*0* indicates initial) |
| $X_{CO2}$ | Fractional $CO_2$ capture, or $CO_2$ chemical conversion |
| $X_C$ | Conversion of carbonate to bicarbonate describes $CO_2$ loading state of $K_2CO_3$ liquid. |
| $X_B$ | Conversion of base B in solution, also written as $X_C$, used to describe $CO_2$ loading state. |
| $y_{A0}$ | Feed gas $CO_2$ mole fraction (subscript *A* represents $CO_2$, *0* indicates initial condition, feed point) |
| $y_A$ | $CO_2$ mole fraction at any point in the absorber, including the exit. |
| $V$ | Packed volume of the reactor ($m^3$, or Liters) |
| $W_{eq,\ Tot}$ | Total equivalent work of $CO_2$ capture (kWh/t $CO_2$), represents total parasitic power impact |

### *1.1. Basic Chemistry*

$CO_2$ is captured into alkaline salt systems via the hydration of dissolved $CO_2$ to form bicarbonate and proton ions in solution. This reaction is known to be very slow without a catalyst, but efficiently catalyzed by carbonic anhydrase enzyme. [9]

$$CO_2 + H_2O \xleftrightarrow{CA} HCO_3^- + H^+ \tag{1}$$

A generic base, $B^-$, functions to capture the proton and complete the reaction:

$$H^+ + B^- \leftrightarrow BH \tag{2}$$

The overall reaction:

$$CO_2 + H_2O + B^- \leftrightarrow HCO_3^- + BH \tag{3}$$

### *1.2. Enzyme Kinetics*

Baird and Sly [9] have reported the molecular weight and turnover number ($k_{cat}$) for human $CA_{IV}$ as 29,800 g/mol and 1.1 per microsecond; the second order rate constant ($k_{cat}/K_M$) = 51 x$10^6$ L/(mol·s) measured at 25°C; and the Michaelis constant, $K_M$, = 21.6 mM. This data can be used to accurately estimate interfacial mass transfer coefficients for dissolved CA using Danckwerts surface renewal model, taking into account the Michaelis-Menten rate law. Soluble enzymes follow the expected trend for reaction enhanced liquid film mass transfer coefficient, in that it is proportional to the square root of the enzyme concentration:

$$\textit{Enhancement Factor:}\quad \frac{\left(k_g^{'}\right)_{cat}}{\left(k_g^{'}\right)_{no\ rxn}} \approx \sqrt{\frac{k_{cat}}{K_M}[E_0]}$$

Accordingly ~0.5 g/L (or about 17 μM) of soluble CA with MW of 30,000 should achieve about 30-fold enhancement in liquid film mass transfer coefficient compared to that without reaction. For comparison, the enhancement factor for 20% $K_2CO_3$ (with no enzyme) at room temperature is approximately 2-fold relative to the physical mass transfer coefficient of a non-reacting fluid.

### *1.3. Immobilized Enzyme Systems*

Akermin uses a sol-gel process to encapsulate CA in an organosilicate matrix, the specifics of which have been described elsewhere [10], [11]. Figure 1 illustrates the basic concept of enzyme encapsulation and delivery.

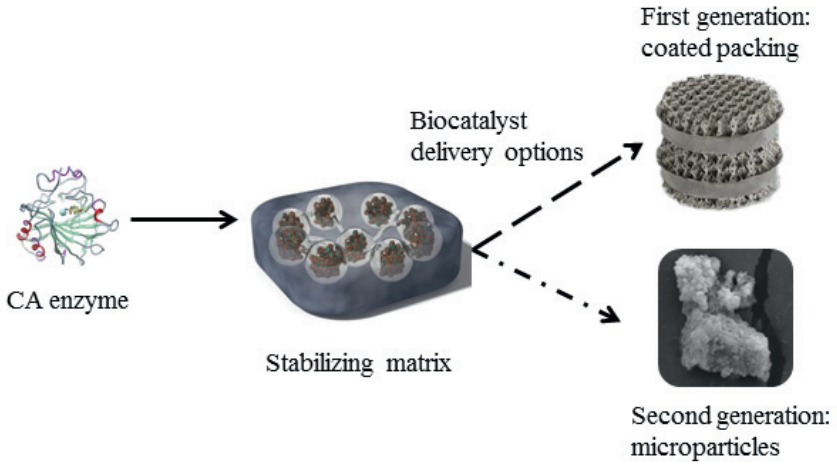


Fig. 1. CA is encapsulated into a stabilizing matrix that can be produced in two delivery options (coated-packing and micro-particles).

The biocatalyst matrix was initially developed as a sol-gel derived coating deposited on stainless steel sheets then assembled into structured packing elements (e.g., Sulzer M500X) for laboratory development and also field demonstration. In the first generation approach, only absorber packing was coated, holding enzyme in fixed position within the absorber column. The intent was to promote the absorption reaction that occurs at lower temperatures in the flue gas application (e.g., 40°C) while avoiding the higher temperature stripper and reboiler systems (e.g., >100°C). In the second generation approach, enzyme was similarly encapsulated within a sol-gel matrix but delivered in the form of a free floating xerogel powder suspension.

It should be recognized that additional diffusional barriers can potentially be introduced by immobilization of catalyst. In liquid systems, solute diffusion in pores of the heterogeneous catalyst relative to diffusion in the bulk liquid is given by the following fourth order estimate [12], Eq 4.

$$\frac{D_{pore}}{D_{bulk}} = \left(1 - \frac{d_s}{d_p}\right)^4 \tag{4}$$

For example, the diffusion diameter of bicarbonate solute ($d_s$) is approximately 0.4 nm, therefore pore diffusion will approach diffusion in the bulk liquid ($D_{pore}/D_{bulk}$ >90%) if average pore size ($d_p$) is greater than 15 nm. This average pore size should be carefully considered while designing the entrapment matrix for the enzyme immobilization.

### *1.4. Considerations for alkali base concentration*

The solubility of the bicarbonate in the rich $CO_2$ loaded solution is an important consideration when defining the alkali salt concentration to be used in a given application. The base system will define the equilibrium rich loading limits, absorption capacity, and precipitation concerns.

For example, if potassium carbonate $K_2CO_3$ is the chosen system, then the proton acceptor for $CO_2$ capture is carbonate ($CO_3^{=}$), in which case two bicarbonate ions will be formed for each $CO_2$ captured. Conversely, only one bicarbonate ion is formed per $CO_2$ captured along with a protonated base in the AKM24 system, which is advantageous from both the equilibrium and the maximum solvent concentration standpoints.

A 20% $K_2CO_3$ concentration (equivalent unloaded) was selected for initial development to give a safe operating margin over the precipitation limits at the maximum rich loading condition (e.g., carbonate conversion $X_C > 0.7$). Eq. 5 presents a correlation for the potassium bicarbonate solubility product constant, $K_{SP}$ (molality basis), based on published data:

$$\ln(K_{SP}) = \ln(m_{K^+} m_{HCO_3^-}) = 11.23 + \frac{2581}{T} \tag{5}$$

## 2. Laboratory Scale Engineering Data

Laboratory vapor-liquid equilibrium and reaction enhanced mass transfer data presented in this section has been used to develop an engineering process model. Potassium carbonate has been well studied by Tosh *et al.* at elevated temperatures with an excellent equilibrium data set available from 70° to 130°C. [13] However, the mass transfer coefficient and vapor-liquid equilibrium data at temperatures relevant to flue gas and laboratory test conditions (23 to 45°C) had to be generated.

### *2.1. Laboratory Reactors and Methods*

Dugas and Rochelle [14] describe a method to quantify equilibrium partial pressures and overall mass transfer coefficients in a wetted wall column. Our work follows a similar principle where feed gas is presented with various $CO_2$ partial pressures at constant flow conditions. Molar rates of $CO_2$ capture are plotted versus average partial pressure in the reactor (log-mean average estimate). The equilibrium partial pressure is determined at the zero $CO_2$ capture rate intersection by linear regression. Key assumptions for wetted wall column testing include:

- 100% area efficiency (due to laminar flow contactor)
- Negligible liquid phase $CO_2$ loading gradients
- Isothermal system
- Average $CO_2$ partial pressure is taken as the log-mean value

These same key assumptions (other than area efficiency) are applicable to a simple packed column reactor operated with high relative liquid circulation rates such that the lean to rich spread is relatively minor. Figure 2 below illustrates the general set-up of laboratory test reactors used in this investigation. Various packing materials were used, including model ceramic spheres and conventional structured packing elements. The liquid flux and gas superficial velocity were held constant for a given series of experiments, keeping the area efficiency and liquid

holdup constant. While interfacial area efficiency ($a_e/a_p$) was not known *a priori*, it could be determined when necessary by comparing mass transfer coefficients to wetted wall column data for standard un-catalyzed solvents (e.g., blank $K_2CO_3$).

A fixed fraction of $CO_2$ blended with air was provided to the system from which a small portion was bled off for continuous analysis by non-dispersive infrared analysis (Quantek-906 NDIR). The feed gas flow rate was held constant using a digital mass flow controller (Alicat MFC) that delivers gas to a controlled temperature saturator. The pressure in the reactor is held constant by a mechanical back pressure regulator (ControlAir-700BP). Outlet $CO_2$ concentrations are also measured using a continuous NDIR (Quantek-906). The gas is analyzed on dry basis, simplifying calculation of $CO_2$ capture.

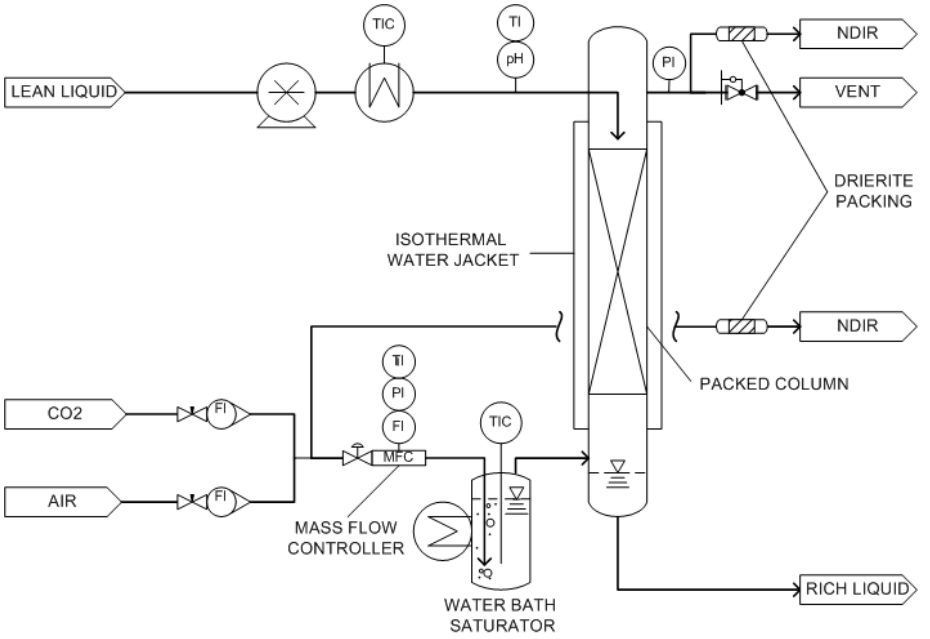


Figure 2. Schematic of laboratory absorber column systems (SPR, TCR, and CLR) used for equilibrium and kinetic studies

### *2.2. Mass transfer coefficients from $CO_2$ capture data*

$CO_2$ capture ($X_{CO2}$) is defined as the chemical conversion of $CO_2$ in the absorption reactor—as indicated in Eq. 6. $CO_2$ capture is calculated using the dry basis $CO_2$ mole fractions at the inlet ($y_{A0}$) and exit ($y_A$):

$$X_{CO_2} \equiv \frac{\Delta F_A}{F_{A0}} = \frac{\left(y_{A0} - y_A\right)}{y_{A0}\left(1 - y_A\right)} \tag{6}$$

The laboratory reactors are analyzed using a plug flow reactor model with a reversible first order rate law [15], where $k_1$ is interpreted as the volume average mass transfer coefficient. Tests are conducted with high liquid to gas ratio so that the equilibrium partial pressure, $C^*_A$, can be assumed constant.

$$\frac{dF_A}{dV} = -k_1 (C_A - C_A^*). \tag{7}$$

The above PFR (plug flow reactor) design equation can be solved in terms of the $CO_2$ capture and integrated over the entire packed volume. The formal analysis accounts for the change in moles in the gas phase that results in two integral terms as shown in Eq. 8, where the space time $\tau = V/v_0$ (or packed volume divided by initial gas volume flow rate).

$$k_1\tau = -\ln\left[\frac{X^*_{CO_2} - X_{CO_2}}{X^*_{CO_2}}\right] - y_{A0}\int_0^{X_{CO_2}} \frac{XdX}{X^* - X}. \tag{8a}$$

The second term is neglected under dilute gas approximation. For typical flue gas conditions with up to 15% $CO_2$ and up to 90% capture, the error in mass transfer coefficient calculation is relatively small. Therefore, Eq. 8b is used in this work to calculate the mass transfer coefficients from measured $CO_2$ capture data and known space time.

$$k_1\tau \approx -\ln\left[\frac{X^*_{CO_2} - X_{CO_2}}{X^*_{CO_2}}\right]. \tag{8b}$$

Under lean test conditions, the equilibrium partial pressure is typically sufficiently low that the equilibrium $CO_2$ capture ($X^*_{CO2}$) will approach unity, therefore Eq. 8 simplifies further:

$$k_1\tau = -\ln\left(1 - X_{CO_2}\right). \tag{9}$$

Therefore, mass transfer coefficients can be related to $CO_2$ capture measurements and known gas space time for any given test condition using either Eq. 8 when $CO_2$ capture may be limited by equilibrium, or Eq. 9 when equilibrium capture approaches unity. Mass transfer enhancement (or 'multiplier') is defined as the ratio of volume average mass transfer coefficients for biocatalyst enhanced system relative to a non-catalyzed baseline reference.

$$M = \frac{(k_1)_{catalyzed}}{(k_1)_{blank}}. \tag{10}$$

Notably, the interfacial mass transfer coefficient can be derived from measurements of volume average mass transfer coefficients using Eq. 11 below—where $\phi_{void}$ is taken as the operational void fraction (dry void fraction less liquid hold up), and $a'_p$ is the packing area density ($m^2/m^3$), and $\eta_e$ is the interfacial area efficiency ($\eta_e = a_e/a_p$).

$$K_{G,I} = \frac{k_1}{\phi_{void}\, a'_P \eta_e RT}. \tag{11}$$

### 2.3. Calibrated pH Assay for $CO_2$ loading

A pH assay technique is used to quantify $CO_2$ loading, which requires concomitant pH and temperature measurements and also knowledge of the solution concentration. The $CO_2$ loading is calculated from calibrated pH and temperature data using the Henderson-Hasselbalch relationship (Eq. 12), where $n$ represents the number of bicarbonate formed per base converted; for example, $n = 2$ for $CO_3^{=}$, while $n = 1$ for bases that form one bicarbonate per $CO_2$ captured. $pK_{a2}$ values are corrected for temperature and ionic strength (salt concentration) using activity coefficient data from Akermin's laboratory; however, mean activity coefficients can also be used where available from the literature [16].

$$X_C = \frac{10^{(pH-pK_{a2})}}{n+10^{(pH-pK_{a2})}} \tag{12}$$

### 2.4. Vapor-Liquid Equilibrium Data

The vapor-liquid equilibrium constant for Equation (3) can be derived from Eq. 13:

$$1/K_{eq} = \frac{[H_2O][B^-]}{[HCO_3^-][BH]} P^*_{CO_2} \tag{13}$$

Figure 3 presents equilibrium data for two alkali salt systems: 20% $K_2CO_3$ and 35% AKM24.

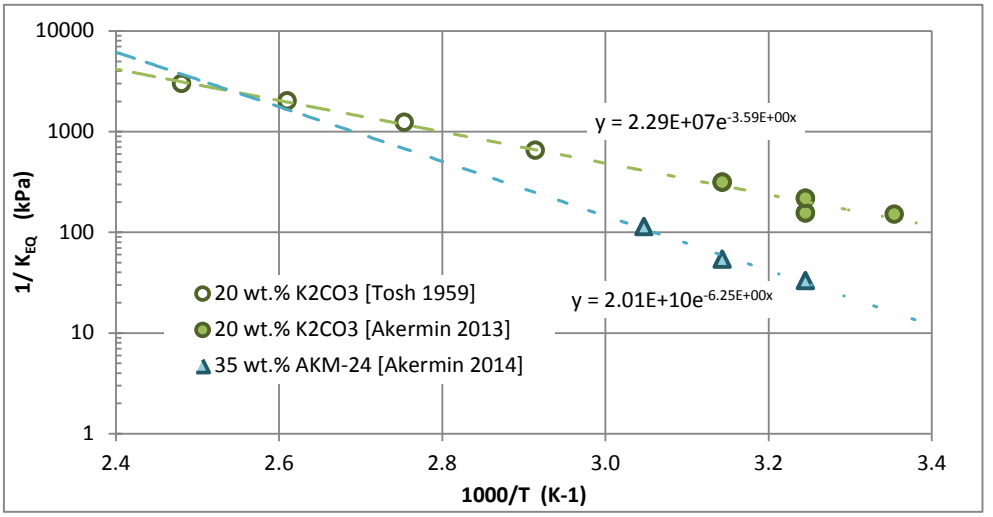


Figure 3. $CO_2$ partial pressure equilibrium constant data for 20% $K_2CO_3$ and 35% AKM24.

Measurements of equilibrium $CO_2$ partial pressure ($P^*_{CO2}$) were made in a 'short packed reactor' (SPR) with approximately 54 ml of model spherical packing (Tipton) configured as shown in Fig. 2, section 2.1 using varied feed gas $CO_2$ partial pressures. [14] $CO_2$ capture rates are measured at a fixed gas flow rate (100 sccm) with varied $CO_2$ partial pressure and fixed liquid flow rate (25 ml/min) for a given $CO_2$ loading and temperature condition. These rate data are plotted against average $CO_2$ partial pressure in the column (log mean average), and equilibrium partial pressure is found at the zero rate intersection. Equilibrium partial pressure data measured in Akermin's laboratory (from 25 to 55°C) and data reported in literature for 20% $K_2CO_3$ (70 to 130°C) are converted to equilibrium constants averaged over various $CO_2$ loading conditions.

Akermin's data fills in the lower temperature region not addressed by Tosh, forming a consistent trend (Fig. 3). It should be noted, however, that extrapolating the Tosh data to lower temperatures over predicts the $CO_2$ partial pressures and under-predicts the heat of reaction. Thus, extrapolating Tosh data to flue gas conditions can lead to errors. More favorable absorption equilibrium for AKM24 at typical flue gas temperatures (40 to 50°C) is apparent from the results presented in Fig. 3. The steeper slope with AKM24 is also indicative of a higher heat of reaction (to be discussed in the next section).

The reaction stoichiometry in Eq. 3 can be used to present concentrations in terms of the initial base concentration and base conversion, $X_C$, as shown in Eq. 14. This expression is used to calculate the equilibrium constant from partial pressure ($P^*_{CO2}$) data. Conversely, the equilibrium expression is useful for predicting $CO_2$ partial pressures in the most accurate way across a wide range of $CO_2$ loading, $X_C$:

$$1/K_{eq} = \frac{[R_{w_0,B_0} - X_C][1 - X_C]}{[X_C]^2} P^*_{CO_2} \tag{14}$$

Where, $R_{w0,B0}$ is the ratio of initial water to initial base (mol water/mol base) in the unloaded state and calculated from the *equivalent* (as unloaded) base mass fraction, $x_0$:

$$R_{w_0,B_0} = \left(\frac{1-x_0}{x_0}\right)\frac{M_{Base\,Salt}}{M_{H_2O}} \tag{15}$$

Data regression yields an expression of the following form in Eq. 16, consistent with theory.

$$K_{EQ} = K_0\left(1 + a\frac{x_0}{1-x_0}\right)e^{-b/T} \tag{16}$$

Correlation coefficients for Eq. 11 programmed into AspenPlus are presented in Table 1.

Table 1. Regression parameters based on theoretical dependencies

| Regression Parameter | $K_2CO_3$ | AKM24 |
|---|---|---|
| b (=-$\Delta H_{abs}/RT^2$) | 35,859 | 62,478 |
| $K_0$ | 1.837E+06 | 7.260E+09 |
| *a* | 2.22 | 0.95 |

### *2.5. Heats of Absorption*

Heat of reaction as a function of temperature can be derived from a Gibbs-Helmholtz analysis of the equilibrium partial pressure data set as described in literature [2]. For the thermally activated process, the heat of reaction relates to the exponential correlation coefficient *b*:

$$\Delta H_{abs} = -bRT^2 . \tag{17}$$

Heat of reaction as a function of temperature was calculated from the partial pressure data using Eq. 17. Figure 4 below compares the heat of reaction for two $CO_2$ capture solutions in this study.

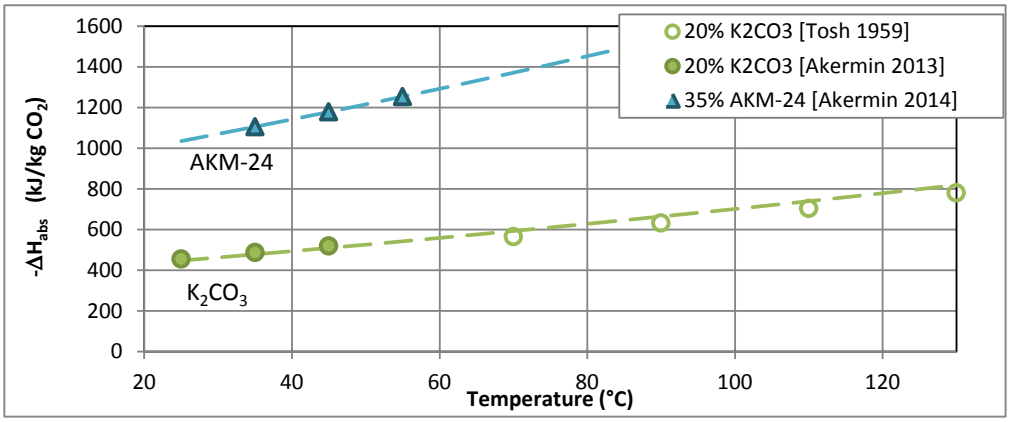


Figure 4. Heat of absorption ($-\Delta H_{abs}$) for $K_2CO_3$ and AKM24 alkali salt systems

The heat of reaction for $CO_2$ absorption into AKM24 is higher than into $K_2CO_3$. Molar heat of absorption for AKM24 at 50°C is approximately 53 kJ/mol $CO_2$ (1200 kJ/kg $CO_2$), which is quite similar to the molar heat of vaporization of water at the same temperature (43 kJ/mol). Notably, the latent duty temperature dependence is governed by the difference between molar heat of reaction and heat of vaporization of water. Therefore, one would expect the reboiler heat duty (specifically the latent duty) to be nearly independent of temperature in a non-kinetically limited regime. This fact is expected to give an added advantage to enable utilization of lower grade heat sources to minimize the parasitic impact of steam extraction for regeneration.

### *2.6. Baseline Rate Data (Laboratory)*

Figure 5 provides a baseline (un-catalyzed) data set for benchmarking biocatalyst enhanced mass transfer data. Baseline $CO_2$ capture data was collected for 20% $K_2CO_3$ and 35% AKM24 solutions using the small packed column reactor (SPR) filled with model spherical random packing. Supporting data tables are provided in the Appendix, Tables A1 and A2.

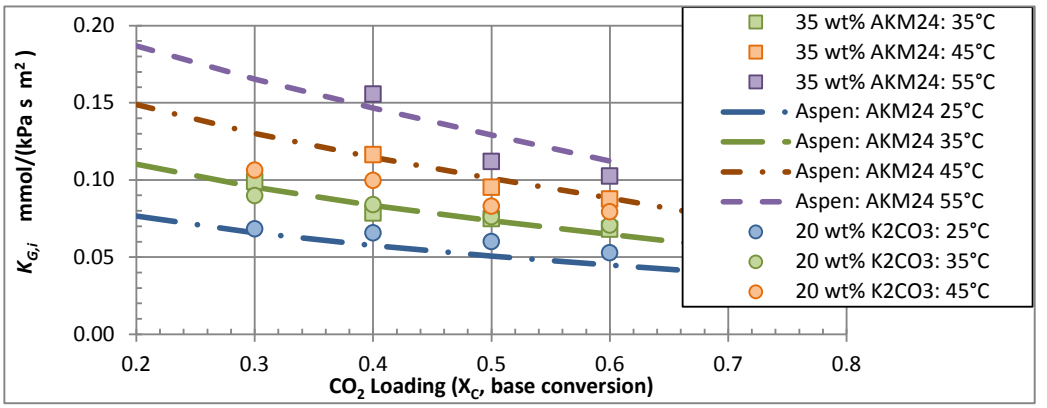


Figure 5. Interfacial mass transfer coefficients for $K_2CO_3$ and AKM24 alkali salt systems

A 'Small Packed Reactor' (SPR) column in arrangement described in Figure 2, section 2.1 is comprised of a clear acrylic column with 15.9 mm inside diameter filled with 65 g of Tipton ceramic packing (7.158 $cm^2/g$, 2.28 $g/cm^3$ solid, 3.66 mm diameter spheres). The packed volume amounts to about 54 ml, which gives a dry void fraction of 47.2%. Gas was fed to the reactor at 100 SCCM with a liquid flow rate of 25 ml/min. Under these conditions liquid hold up was 13.3% and the wet operating void fraction was 33.9%. By comparing mass transfer coefficients for $K_2CO_3$ on a packing area basis to wetted wall column data, the interfacial area relative to packing area ($a_e/a_p$) was estimated to be about 30% (relative to 861 $m^2/m^3$ packing area).

*2.7. Biocatalyst Enhanced Data (Laboratory)*

Figure 6 presents the volume average mass transfer coefficient for a second generation biocatalyst sample as a function of biocatalyst concentration. Mass transfer coefficients with varied amounts of second generation biocatalyst was studied in a 54 mm ID x 2.67 m 'Tall Column Reactor' (TCR) containing 6.1 Liters of M500X packing (360 $m^2/m^3$ packing due to small ID of column) using the arrangement described in Figure 2, section 2.1. The interfacial area relative to packing area ($a_e/a_p$) of this column was estimated to be about 24.2%. The wet operating void fraction was 78% and the liquid holdup was 20%.

Gas is fed to the TCR at 30 SLPM with about 15% $CO_2$ and 3 LPM liquid circulation at 40°C and 0.3 mol/mol $CO_2$ loading. In this experiment, biocatalyst concentrations began at zero to establish a baseline and then three separate doses of Gen-2A biocatalyst (enzyme containing micro-particles) were added until a total of 0.34 wt% biocatalyst was achieved in suspension. $CO_2$ capture data was collected at each biocatalyst concentration. A similar test was performed with fresh solution where Gen-2B biocatalyst was subsequently added to 0.75 wt%. Supporting data tables are provided in the Appendix, Table A3.

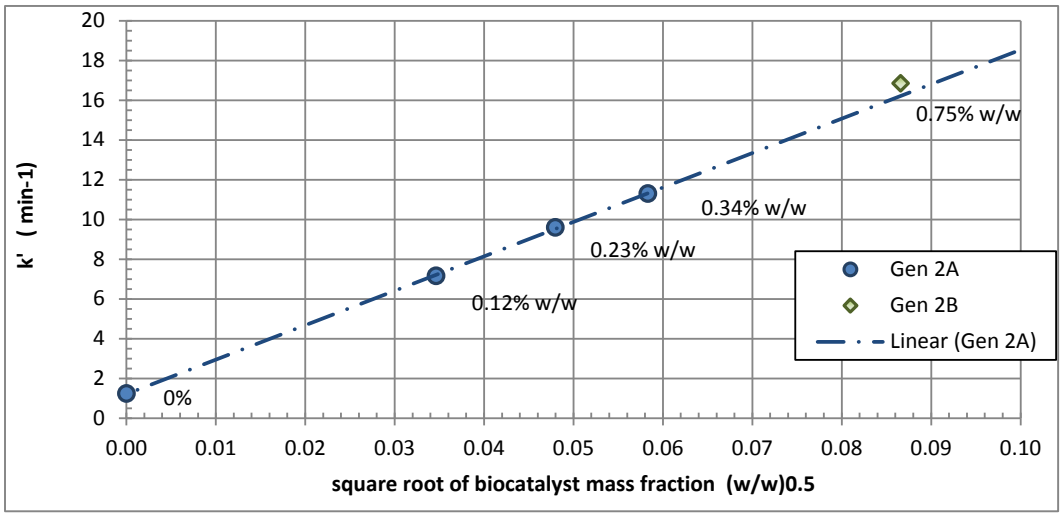


Figure 6. Volume average mass transfer coefficients for Gen 2A and 2B biocatalyst in TCR with AKM24, 0.3 $X_C$, 40 °C.

The mass transfer coefficients presented in Fig. 6 show a characteristic square root dependence on biocatalyst concentration, consistent with Danckwerts surface renewal theory. Gen-2B biocatalyst with 0.75% w/w concentration achieved $k'$ = 16.8/min with AKM24 in the TCR at 40°C—which is 13.6-fold higher than the same solution without catalyst (blank $k'$ = 1.24/min at 40°C), and 25.8-fold higher than its room temperature blank ($k'$ = 0.65/min at 25°C). For the purpose of benchmarking to previous work, the rate performance of Gen-2B in the TCR system was 22.4 fold higher than 20% $K_2CO_3$ at 25°C, 0.3 $X_C$ ($k'$ = 0.75/min at *RT*).

Additional testing is planned to confirm the square root dependence especially when achieving high overall enhancement factors. Since the biocatalyst performance is driven by its concentration near the gas-liquid interface, the enhancement will eventually reach a practical limit. Also, gas film resistance will begin to play a more important role in the overall mass transfer coefficient trend at high enhancement factors. Still, the 25.8-fold enhancement of the overall mass transfer coefficient over room temperature AKM24 rivals the performance of lean 30% MEA at 40°C.

Figure 7 provides a comparison of relative enhancement factors (normalized to potassium carbonate at room temperature) for first generation biocatalyst (coating) and second generation biocatalyst (micro-particles) systems in comparison with 30% MEA at 40°.

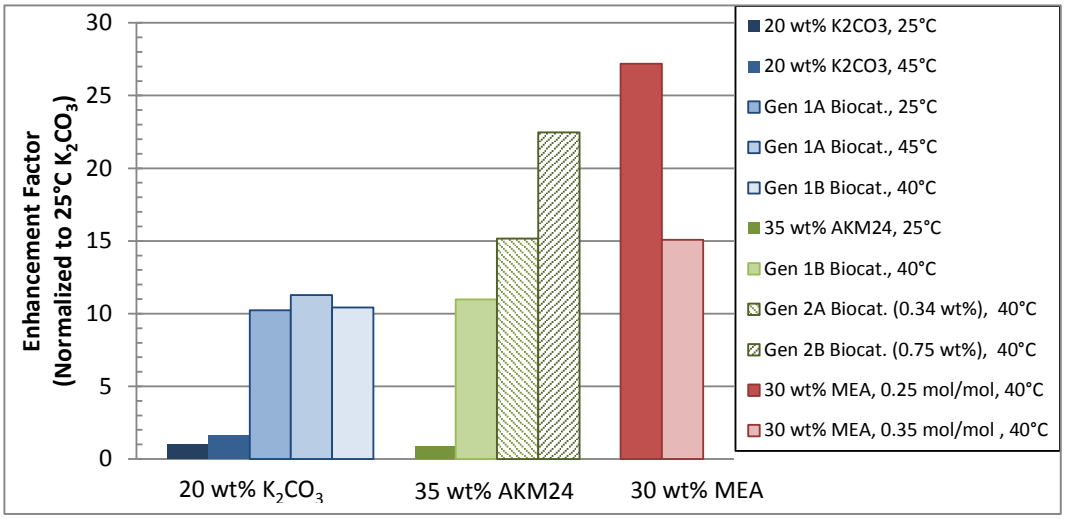


Figure 7. Enhancement factor for Gen-1 and Gen-2 biocatalysts and MEA relative to 20% $K_2CO_3$ at 0.3 $X_C$, 25°C.

Clearly, there is a superior enhancement potential with the second generation biocatalyst delivery system over the first generation approach considering that the performance of a suspension with as low as 0.34% w/w biocatalyst exceeds that of 30% MEA at 40 $^oC$ and 0.35 mol/mol $CO_2$ loading. Moreover, 1% biocatalyst is projected to rival lean MEA performance (30% w/w at 0.25 lean loading).

## 3. Field Test Data

### *3.1. System Description*

The NETL-Akermin field test unit installed and operated at the National Carbon Capture Center in Wilsonville Alabama included an absorber containing 36 layers each of 205 mm ODE x 222-mm tall M500X packing installed in a 211-mm ID pipe operated with an L/G of 7.88 kg/kg at the design point.

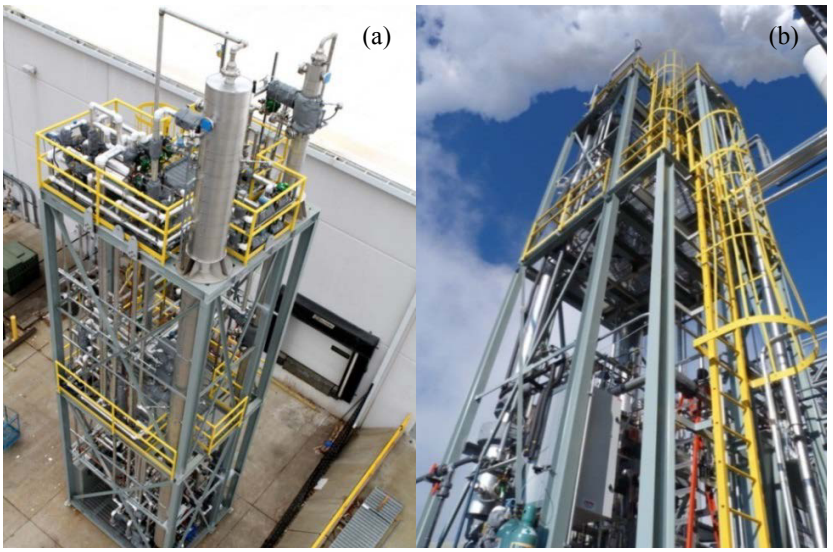


Figure 8. (a) NETL-Akermin field unit in fabrication (stripper in foreground and absorber in background). (b) NETL-Akermin field unit installed at the National Carbon Capture Center, Wilsonville AL showing steam and flue gas tie-in on right hand side.

### *3.2. Rate Data*

The field test absorber column had the following characteristics: an area efficiency of ~10.5% (relative to 420 $m^2/m^3$ total packing area) and a wet operating void fraction of 88.5%. Fig. 9b demonstrates a clear rate enhancement in $CO_2$ capture by the enzyme compared to blank. The improvement in volumetric average mass transfer coefficient is quantified by comparing the slope of the first order rate plot in Fig. 9(b)—which indicates about 6-fold improvement with 40°C lean solution feed. When normalized to room temperature reference, the Gen-1B biocatalyst sample exhibited about 10-fold enhancement.

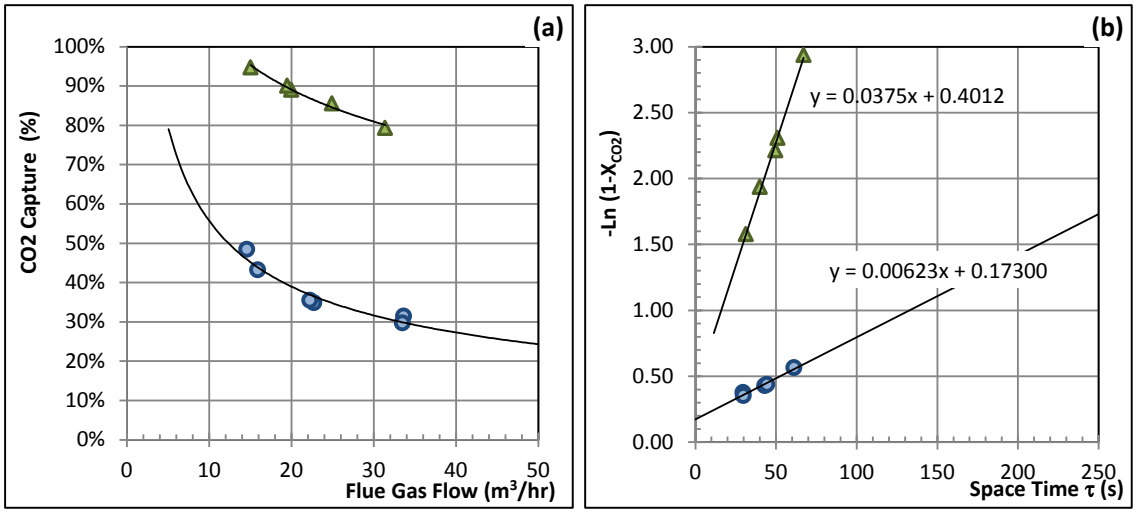


Figure 9. (a) $CO_2$ capture data for Gen-1B biocatalyst in the NETL-Akermin field test unit at NCCC. (b) First order plots that indicate 6-fold increase in slope (or 6X increase in volume average mass transfer coefficient).

Indeed, 90% capture was achieved with approximately 20.1 $Nm^3$/hr gas flow rate (19.5 $Nm^3$/hr dry basis) using biocatalyst-coated packing. In contrast, data trends indicate that 90% capture would be achieved at as low as 2.8 $Nm^3$/hr gas flow (about 2.7 $Nm^3$/hr dry) with the same liquid-to-gas (L/G) ratio in the absence of the biocatalyst. In other words, a 7-fold increase in gas flow rate can be processed to 90% capture in the same column volume when using the Gen-1B biocatalyst sample.

In addition to testing mentioned above, long-term endurance testing was conducted to demonstrate the reliability of the system's performance and longevity of the Gen-1B biocatalyst (Fig. 10). The system was run for a total of about 6 months (5 months utilizing $K_2CO_3$ and 1 month on AKM24) with continuous recirculation of the liquid to the absorber at 40°C and 0.3 mol/mol lean loading. While $CO_2$ concentration was varied by the power plant to support other system testing, the liquid circulation rate and gas flow were held constant throughout the test period.

The results presented in Fig 10 demonstrate that following the first 100 hours the system was operated at steady state and continued in that manner for the next 3400 hr with average $CO_2$ capture in the range of ~ 80%. Quantitative treatment of the entire set of data revealed that the Gen 1B biocatalyst half-life (defined as the length of time on stream during which for the volume average mass transfer coefficient is expected to decrease by half) was about 539 days. It is worth emphasizing that the stability of the catalyst was exceptionally high in both solvents tested.

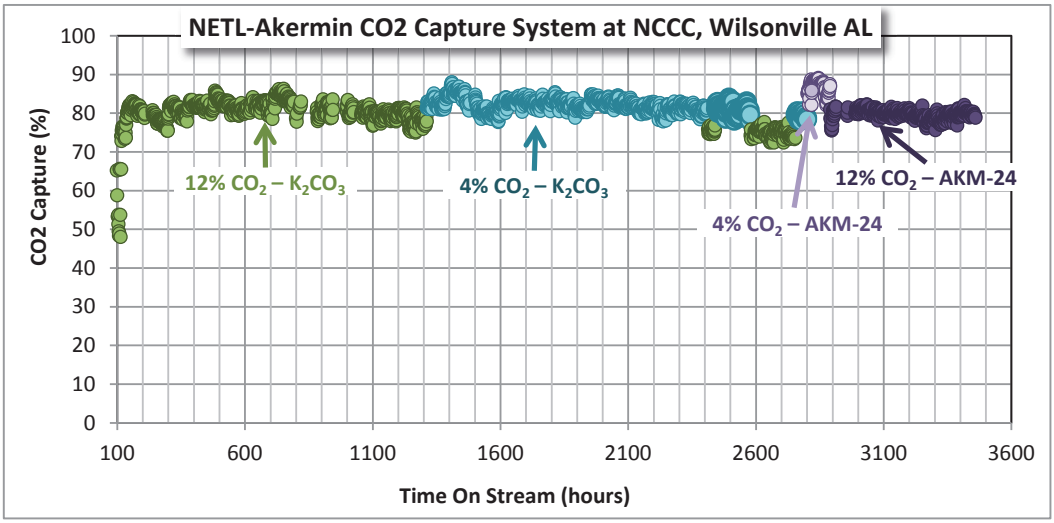


Figure 10. $CO_2$ capture with time indicates stable performance

### *3.3. Energy Observations*

Parametric testing in the NETL-Akermin field test unit with Gen-1B biocatalyst in the absorber (no catalyst in the stripper) was performed to understand the stripper column performance and reboiler heat duty as a function of stripper/reboiler pressure, especially under vacuum conditions. The field data indicated that reboiler duty decreased with decreasing temperature from 105°C down to a minimum energy at about 80°C; below that level, the reboiler heat duty increased with decreasing temperature. [17] This trend was attributed to an increasing kinetic limitation when operating the reboiler and stripper below 80°C and the trend was matched by the Aspen model predictions within 3%. [17]

AspenPlus® (v8.4) models initially developed for $K_2CO_3$ were later adapted to AKM24 based on the equilibrium constant data presented in this paper. In addition, Michaelis-Menten kinetic models for *soluble* enzyme enhanced

$CO_2$ hydration and dehydration were programmed into Aspen using FORTRAN coding. The model predictions of equilibrium and reaction enhanced mass transfer were further validated by comparing with laboratory data.

The Aspen model was used to study the possible benefit of adding biocatalyst to the stripper (as well as to the absorber) enabling lower temperature stripping. The economic driver for lower temperature regeneration is two-fold: (1) to reduce reboiler heat duty in low heat of reaction solvents, and (2) to reduce the total equivalent work (parasitic impact of steam extraction) by using lower grade heat sources for regeneration. (Equivalent work results are discussed further in section 4). Figure 11 presents the Aspen reboiler heat duty predictions performed for four scenarios: (a) blank 20 wt.% $K_2CO_3$, (b) 15X enhanced 20 wt.% $K_2CO_3$, (c) blank AKM24, and (d) 15X enhanced AKM24. The '15X' enhancement refers to the level of mass transfer enhancement that would be observed in a standard laboratory test. It equates to the actual performance of about 0.5 g/L of soluble CA from Novozymes.

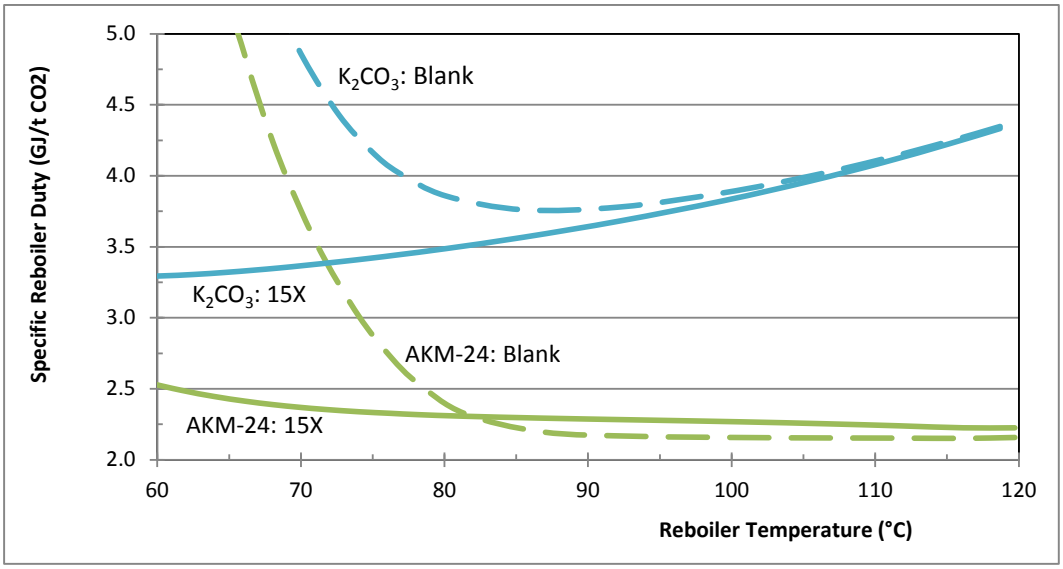


Figure 11. Specific reboiler duty versus regeneration temperature

Figure 11 demonstrates that by accelerating the reverse reaction (i.e., dehydration of bicarbonate), and thereby overcoming kinetic limitations in a lower temperature stripper, the biocatalyst has the potential to reduce the reboiler duty and enables leveraging of low grade heat sources.

## 4. Process Economics

### *4.1. Process Configurations*

By evaluating various system configurations for the first generation biocatalyst utilizing $K_2CO_3$ we found that the most optimal case was a vacuum assisted regeneration with a reboiler operating at 85°C. The focus of this study was to evaluate the process economics of the second generation biocatalyst using AKM24. The economic analysis presented herein assumes about 15-fold enhancement (demonstrated with 0.34% biocatalyst) relative to room temperature capture with $K_2CO_3$. Three cases were selected for economic evaluation: a deep vacuum regeneration case with similar absorption-desorption temperatures (Case-1A), a vacuum assisted regeneration case with an 80°C reboiler (Case-2A), and an ambient pressure regeneration case with a 105°C reboiler (Case-2B).

### 4.2. Equivalent Work Estimates

In power plant post-combustion $CO_2$ capture applications the loss in power from $CO_2$ capture operations can be quantified by the "total equivalent work" of $CO_2$ capture (kWh/t $CO_2$). Equivalent work considers the impact of steam extracted from the turbine power cycle for solvent regeneration instead of being used to produce power (Eq. 19) and the major electrical loads for fans, pumps and $CO_2$ compression (Eq. 18). To calculate reboiler heat duty we used Eq. 19 validated in heat cycle modeling by Van Wagener *et. al*. [18], and assumed the cold reference temperature of 38.42°C as specified in NETL in the Bituminous Baseline Report [19]. Total equivalent work estimates were prepared for four biocatalyst enhanced capture systems (Figure 12) with varied steam extraction temperatures and compared to the commonly accepted 30% MEA reference from the NETL Bituminous baseline report, Case 12 version 2 (291°C steam extraction).

$$W_{Equiv.Total} = W_{ID\,Fan} + W_{Circ.Pumps} + W_{Vac.Blower} + W_{Comp.} + W_{Reboiler} \tag{18}$$

$$W_{Reboiler} = 0.88 Q_{Reboiler}\left(1 - \frac{38.42 + 273.15}{T_{Reboiler,K} + 10}\right) \tag{19}$$

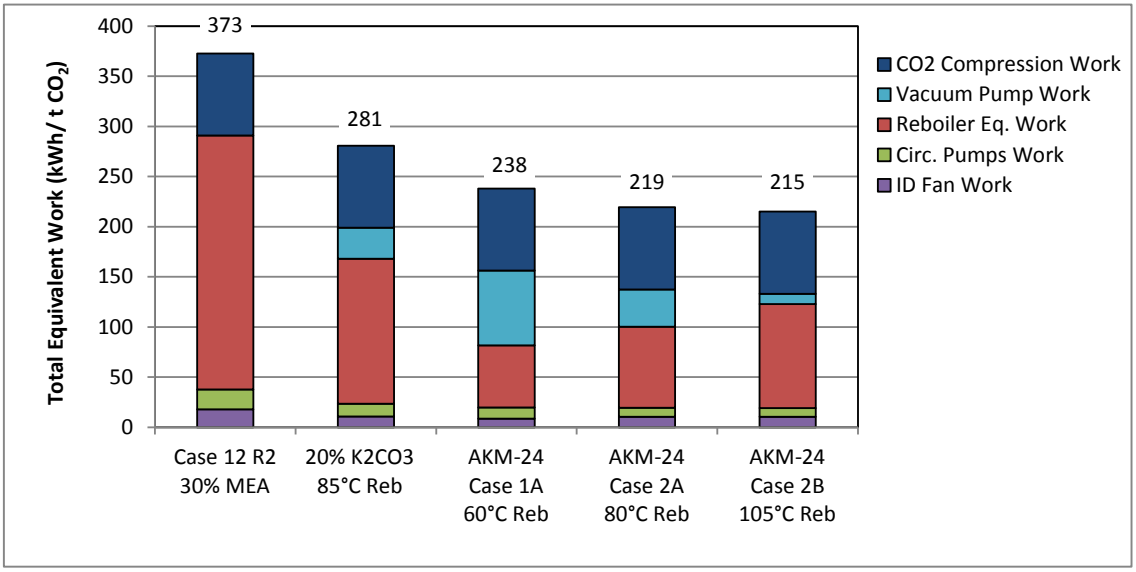


Figure 12. Comparison of total equivalent work for various capture systems

The total equivalent work for Case 12 was quantified to be 373 kWh/t$CO_2$. The primary contributor was the reboiler equivalent work, which accounted for 254 kWh/t$CO_2$. The power required for $CO_2$ compression from 1.6 to 152.7 bara equals to 81.8 kWh/t$CO_2$ and is uniform for all cases.

As Fig. 12 illustrates, reboiler equivalent work for AKM24 cases decreased with decreasing reboiler temperature as lower grade steam is utilized in regeneration due to the beneficial impact of catalyst in the stripper. Case-1A and Case-2A had total equivalent work values of 238 and 219 kWh/t$CO_2$, respectively, each representing considerable reductions relative to Case 12. The analysis also shows that Case-2B (which has the ambient pressure stripper without catalyst) had the lowest total equivalent work requirement of 215 kWh/t$CO_2$, or 42.4% less than Case 12.

### 4.3. Incremental Cost of Electricity

The incremental cost of electricity (ICOE), defined as the net cost of electricity over and above the cost of electricity with no capture, is directly related to the cost of $CO_2$ capture. The no capture reference is NETL Case 11 in the bituminous baseline report [19], which has a delivered electricity price of $80.94/MWh. Figure 13 presents the ICOE for the various capture systems evaluated in this study compared to NETL Case-12 version 2.

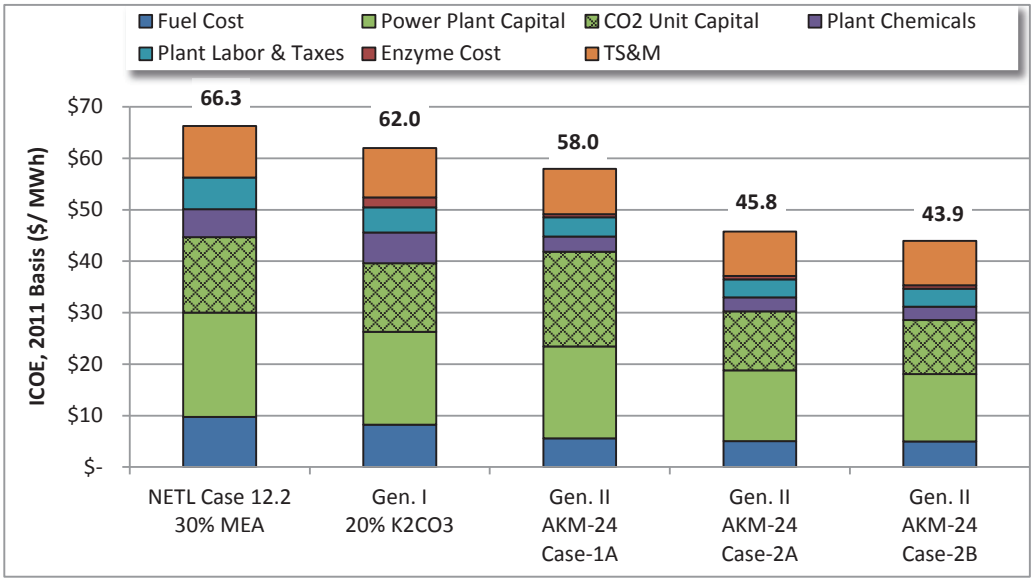


Figure 13. Incremental cost of electricity (ICOE) for various capture systems relative to NETL Case-11 (no capture)

While the first generation (Gen-I) biocatalyst system utilizing $K_2CO_3$ demonstrated only a 6.5% reduction in ICOE relative to Case 12, the second generation systems (Gen II) utilizing AKM24 show more significant potential for cost savings. The best case is the combination of Gen II biocatalyst with ambient pressure $CO_2$ stripping, which demonstrates a 33.8% reduction in ICOE (Case-2B) by this preliminary techno-economic assessment. In this case it was assumed that some form of particle filtration and catalyst recovery was implemented to prevent biocatalyst from entering the stripper and reboiler at 105°C. Alternatively, Case-1A and Case-2A with ICOE cost savings of 12.5% and 30.9% respectively assume that the biocatalyst microparticles circulate freely throughout the entire system. Future work will incorporate results from field testing of the Gen-II biocatalyst system to validate model predictions and cost savings.

## 5. Conclusions

This work has discussed research and development progress to improve biocatalysts, solvents, and system integration to reduce the cost of $CO_2$ capture from flue gas and obviate the risk of VOC and toxic HAP emissions associated with more conventional volatile amine solvents.

Two generations of biocatalyst delivery technology were discussed—biocatalyst coated packing and biocatalyst micro-particle. The field testing of the first generation biocatalyst technology (coated packing) demonstrated 6 to 7-fold enhancement in volume average mass transfer coefficient at 40°C (equivalent to 10-fold enhancement over blank at 22 $^{O}$C).

The second generation biocatalyst (micro-particle) offers a greater potential for rate enhancement compared to the first generation technology (coated packing). For example, at 0.34 w/w % biocatalyst loading in AKM24, the

mass transfer enhancement was 15-times that of a standard room temperature reference, which approaches 30% MEA at 40°C. Data shows that >20X enhancement is possible with modest biocatalyst concentration, and development continues to improve this catalyst system.

Moreover, the longest and the largest scale public demonstration of enzyme enhanced $CO_2$ capture from flue gas was presented with the first generation biocatalyst technology at the National Carbon Capture Center demonstrating 3460 hours on coal flue gas with average 80% $CO_2$ capture. Notably, the biocatalyst stability was demonstrated for both $K_2CO_3$ and a non-volatile alkaline salt solution, AKM24.

Finally, modeling indicates realistic potential to reduce total equivalent work of $CO_2$ capture in a coal power plant application to less than 220 kWh/t$CO_2$. Configurations presented in this paper achieved as much as 42% reduction in equivalent work based on AspenPlus modeling versus NETL Case 12, version 2. Significant savings in the incremental cost of electricity was also demonstrated, indicating a pathway to achieve more than 30% reduction in cost of electricity versus NETL Case 12 version 2. Future work is expected to lead to even higher enhancement factors with biocatalyst particle and longer-term stability at the desired operating conditions.

Future work to advance this technology includes:

- Further optimization of the biocatalyst,
- Demonstration of performance and advanced process configurations at next scale,
- Development of low energy process configurations using the data validated process model,
- Further cost reduction with 20X enhancement factors demonstrated in laboratory,
- Waste heat integration (for example, from $CO_2$ compression system) to further reduce the equivalent work of $CO_2$ capture from steam-power plants.

## Acknowledgements

This paper is based upon work supported by the Department of Energy National Energy Technology Laboratory under Award Numbers DE-FE0004228 and DE-FE0012862. Akermin also acknowledges Novozymes for their generous supply of active carbonic anhydrase enzymes for this project.

## Disclaimer



## Appendix A. Mass Transfer Data Tables

SPR baseline data (15.9 mm ID x 54 ml total volume, 3.66 mm spherical ceramic packing by Tipton) supporting Figure 5 is presented in Tables A1 and A2.

Table A1. SPR Baseline Rate Data with 20 wt% $K_2CO_3$

| $T$ (°C) | $X_C$ | $X_{CO2}$ | $X^*$ | $\tau = V/v_0$ (second) | $k'$ (1/min) | $K_{G,I}$ (mmol/ (kPa s m$^2$) |
|---|---|---|---|---|---|---|
| 25 | 0.3 | 37.9% | 96.2% | 34.1 | 0.88 | 0.068 |
| 25 | 0.4 | 36.9% | 96.5% | 34.1 | 0.85 | 0.066 |
| 25 | 0.5 | 33.5% | 94.1% | 34.1 | 0.78 | 0.060 |
| 25 | 0.6 | 29.8% | 93.0% | 34.1 | 0.68 | 0.053 |
| 25 | 0.7 | 25.9% | 85.3% | 34.1 | 0.64 | 0.049 |
| 35 | 0.3 | 43.2% | 93.4% | 33.0 | 1.13 | 0.090 |
| 35 | 0.4 | 41.9% | 91.1% | 33.0 | 1.12 | 0.084 |
| 35 | 0.5 | 36.7% | 85.8% | 33.0 | 1.02 | 0.076 |
| 35 | 0.6 | 32.9% | 81.1% | 33.0 | 0.94 | 0.071 |
| 35 | 0.7 | 22.8% | 64.4% | 33.0 | 0.79 | 0.060 |
| 45 | 0.3 | 49.5% | 91.4% | 31.9 | 1.47 | 0.106 |
| 45 | 0.4 | 44.9% | 86.5% | 31.9 | 1.37 | 0.100 |
| 45 | 0.5 | 37.1% | 81.4% | 31.9 | 1.14 | 0.083 |
| 45 | 0.6 | 31.4% | 71.2% | 31.9 | 1.09 | 0.079 |
| 45 | 0.7 | 20.5% | 48.6% | 31.9 | 1.03 | 0.075 |

Table A2. SPR baseline rate data for 35% AKM24

| $T$ (°C) | $X_C$ | $X_{CO2}$ | $X^*$ | $\tau = V/v_0$ (second) | $k'$ (1/min) | $K_{G,I}$ (mmol/ (kPa s m$^2$) |
|---|---|---|---|---|---|---|
| 35 | 0.4 | 42.9% | 96.7% | 33.0 | 1.01 | 0.078 |
| 35 | 0.5 | 39.4% | 92.0% | 33.0 | 0.97 | 0.075 |
| 35 | 0.6 | 34.0% | 85.2% | 33.0 | 0.88 | 0.068 |
| 35 | 0.7 | 30.6% | 78.7% | 33.0 | 0.85 | 0.066 |
| 45 | 0.4 | 53.1% | 91.5% | 31.9 | 1.50 | 0.116 |
| 45 | 0.5 | 42.7% | 83.9% | 31.9 | 1.23 | 0.095 |
| 45 | 0.6 | 30.2% | 62.9% | 31.9 | 1.13 | 0.088 |
| 35 | 0.3 | 51.2% | 97.9% | 33.0 | 1.28 | 0.099 |
| 55 | 0.4 | 60.0% | 87.3% | 31.0 | 2.01 | 0.156 |
| 55 | 0.5 | 42.8% | 75.6% | 31.0 | 1.44 | 0.112 |
| 55 | 0.6 | 28.6% | 53.4% | 31.0 | 1.32 | 0.102 |

TCR data supporting Figure 6 second generation biocatalyst testing is presented in Tables A3. The TCR system is comprised of a 54 mm ID x 2.67 m packed column, or 6.1 Liters of M500X packing (360 m$^2$/m$^3$ packing due to small ID of column). The TCR system employs an arrangement similar to that described in Figure 2, section 2.1.

Gas is feed to the TCR at 30 SLPM with about 15% $CO_2$ and 3 LPM liquid circulation at 40°C and 0.3 mol/mol $CO_2$ loading. The interfacial area relative to packing area ($a_e/a_p$) of this column was estimated to be about 24.2% under the typical test conditions. The wet operating void fraction was 78% and the liquid holdup was 20%.

Table A3. TCR data for Gen-2 biocatalyst (micro-particle). Gen-2 (Sample A) = LW-A00167-7; Gen-2 (Sample B) = TB-A00162-67.

| Description | $T$ (°C) | Solution | $X_C$ | $X_{CO2}$ | $X^*$ | $\tau = V/v_0$ (second) | $k'$ (1/min) | Relative Enhancement (over 25°C $K_2CO_3$) |
|---|---|---|---|---|---|---|---|---|
| Blank | 25°C | 20% $K_2CO_3$ | 0.25 | 14.1% | 98.0% | 12.5 | 0.75 | 1 |
| Blank | 25°C | 35% AKM24 | 0.3 | 12.6% | 99.3% | 12.5 | 0.65 | 0.87 |
| Gen-2 (Sample A), 0.12% | 40°C | 35% AKM24 | 0.31 | 72.5% | 97.9% | 11.9 | 6.79 | 9.05 |
| Gen-2 (Sample A), 0.23% | 40°C | 35% AKM24 | 0.32 | 81.4% | 97.5% | 11.9 | 9.05 | 12.06 |
| Gen-2 (Sample A), 0.34% | 40°C | 35% AKM24 | 0.40 | 85.5% | 95.6% | 11.9 | 11.1 | 15.08 |
| Gen-2 (Sample B), 0.75% | 40°C | 34% AKM24 | 0.38 | 83.4% | 96.4% | 7.2 | 16.8 | 22.46 |
| 30% MEA (1) | 40°C | 30% MEA | 0.25 | - | - | - | 20.28 | 27.18 |
| 30% MEA (1) | 40°C | 30% MEA | 0.35 | - | - | - | 11.24 | 15.07 |

(1): $k_l$ calculated using literature reported values for interfacial mass transfer coefficients for MEA: 1.93 mmole/kPa/s/$m^2$ for 0.25 mol/mol $CO_2$ loading, and 1.07 mmole/kPa/s/$m^2$ for 0.35 mol/mol $CO_2$ loading. [14]

Closed loop reactor (CLR) data supporting Figure 7 is presented in Table A4 below. CLR tests utilized a 2.125" ID absorber column that contains 2 layers of Sulzer M500X equating to a volume of about 1.0 liter. Gas is feed to the reactor at 4.36 SLPM (dry basis) with about 15% $CO_2$, and the liquid flow rate was 0.218 LPM. This column utilizes 14.8% of 360 $m^2/m^3$ specific area with a (wet) void fraction of 88.5%, based on liquid hold up of 10%.

Table A4. CLR Blank and Gen-1 Coated Packing Tests. Gen-1 (Sample A) = BMR-3-92 on 50-mm M500X.

| Description | $T$ (°C) | Solution | $X_C$ | $X_{CO2}$ | $X^*$ | $\tau = V/v_0$ (second) | $k'$ (1/min) | Relative Enhancement (over 25°C $K_2CO_3$) |
|---|---|---|---|---|---|---|---|---|
| Blank | 25°C | 20% $K_2CO_3$ | 0.24 | 9.2% | 98.7% | 14.8 | 0.4 | 1 |
| Blank | 45°C | 20% $K_2CO_3$ | 0.23 | 13.5% | 96.7% | 13.8 | 0.65 | 1.63 |
| GEN 1 (sample A) | 25°C | 20% $K_2CO_3$ | 0.22 | 63.1% | 99.5% | 14.6 | 4.09 | 10.23 |
| GEN 1 (sample A) | 45°C | 20% $K_2CO_3$ | 0.22 | 64.2% | 98.8% | 13.8 | 4.51 | 11.28 |

## References


[1] Kohl AL, Nielsen RB. Gas Purification. 5th ed. Houston: Gulf Professional Publishing; 1997.

[2] Oexmann J, Kather A. Minimising the regeneration heat duty of post-combustion CO2 capture by wet chemical absorption: The misguided focus on low heat of absorption solvents. Int. J. of Greenhouse Gas Control. 2010; 4: p. 36-43.

[3] Gjernes E, Helgesen LI, Maree Y. Health and environmental impact of amine based post combustion CO2 capture. In Energy Procedia (GHGT-11); 2013; Kyoto: Elsevier.

[4] Scottish Environmental Protection Agency. Review of Amine Emissions from Carbon Capture Systems. Stirling, UK:; 2013.

[5] Shao R, Stangeland A. Amines Used in CO2 Capture - Health and Environmental Impacts. Oslo, Norway:; 2009.

[6] Wen H, Narula R. Impacts of Carbon Capture on Power Plant Emissions. In Presentation to 12th Meeting of the International Post Combustion Capture Network; 2009; Regina, Canada.

[7] Berglen TF. Norwegian Institute for Air Research. [Online].; 2012 [cited 2012 September. Available from: http://www.klif.no/nyheter/dokumenter/tcm_soknad_vedlegg8.pdf.

[8] Carter T. National Carbon Capture Center: Post Combustion. In 2012 NETL CO2 Capture Technology Meeting; 2012; Pittsburgh: National Energy Technology Laboratory.

[9] Baird TT, Waheed A, Okuyama T, Sly WS, Fierke CA. Catalysis and Inhibition of Human Carbonic Anhydrase IV. Biochemistry. 1997: p. 2669-2678.

[10] Rambo BM, Bucholz TL, Powell DC, Weber LE, Linder AJ, Duesing CMH, et al., inventors; Polysilicate-polysilicone enzyme immobilization materials. US patent 20130267004.

[11] Bucholz TL, Pulvirenti DC, Rambo BM, Hulvey MK, Weber LE, Reardon JP, et al. Development and demonstration of a carbonic anhydrase-containing coating for removal of CO2 from coal-fired flue gas. Energy and Environmental Science. Submitted.

[12] Harriot P. Chemical Reactor Design New York: Marcel Dekker, Inc.; 2003.

[13] Tosh JS, Field JH, Benson HE, Haynes WP. Equilibrium Study of the System Potassium Carbonate, Potassium Bicarbonate, Carbon Dioxide, and Water. Washington: Bureau of Mines, U.S. Department of the Interior; 1959.

[14] Dugas RE, Rochelle GT. CO2 Absorption Rate into Concentrated Aqueous Monoethanolamine and Piperazine. Journal of Chemical & Engineering Data. 2011: p. 2187-2195.

[15] Fogler SH. Elements of Chemical Reaction Engineering. 2nd ed. Englewood Cliffs: Prentice-Hall, Inc.; 1992.

[16] Aseyev GG, Zaytsev ID. Volumetric Properties of Electrolyte Solutions: Estimation Methods and Experimental Data New York: Begell House; 1996.

[17] Reardon J. Advanced Low Energy Enzyme-Catalyzed Solvent for CO2 Capture. In 2013 NETL CO2 Capture Technology Meeting; 2013; Pittsburgh: National Energy Technology Laboratory.

[18] Van Wagener DH, Liebenthal U, Plaza JM, Kather A, Rochelle GT. Maximizing coal-fired power plant efficiency with integration of amine-based CO2 capture in greenfield and retrofit scenarios. Energy. 2014 June: p. 824-831.

[19] National Energy Technology Laboratory. Cost and Performance Baseline for Fossil Energy Plants Volume 1: Bituminous Coal and Natural Gas to Electricity, Revision 2. National Energy Technology Laboratory; 2010. Report No.: DOE/2010/1397.

[20] US Environmental Protection Agency. Operating Permits. [Online].; 2013 [cited 2014 September 3. Available from: http://www.epa.gov/oaqps001/permits/obtain.html.

[21] Danckwerts PV. Gas Absorption Accompanied by Chemical Reaction. A.I.Ch.E. Journal. 1955 December: p. 456-463.

[22] Hilliard MD. A Predictive Thermodynamic Model for Aqueous Blend of Potassium Carbonate, Piperazine, Monoethanolamine for Carbon Dioxide Capture from Flue Gas. PhD Thesis. Austin: University of Texas at Austin; 2008.

[23] Mohammad ARM, Schneiders LHJ, Niederer JPM, Feron PHM, Versteeg GF. CO2 capture from power plants Part I. A parametric study of the technical performance based on monoethanolamine. International Journal of Greenhouse Gas Control. 2006 December: p. 37-46.

[24] Salmon S. Low-Energy Solvents for CO2 Capture Enabled by a Combination of Enzymes and Vacuum Regeneration. In 2014 NETL CO2 Capture Technology Meeting; 2014; Pittsburgh. p. 26.